Int. J. Electrochem. Sci., 2 (**2007**) 82 - 92

International Journal of ELECTROCHEMICAL SCIENCE
www.electrochemsci.org

Hydrogen Diffusivities and Concentrations in 520M Carbon Steel under Cathodic Protection in 0.5M NaCl and the Effect of Added Sulphite, Dithionite, Thiosulphate, and Sulphide

E. Hörnlund, J.K.T. Fossen, S. Hauger, C. Haugen, T. Havn and T. Hemmingsen[*]

University of Stavanger, 4036 Stavanger, Norway
[*]E-mail: tor.hemmingsen@uis.no

Received: 14 December 2006 / *Accepted:* 16 December 2006 / *Published:* 1 January 2007

Hydrogen diffusion experiments in 520M carbon steel were performed with the Devanathan-Statchurski permeation cell at 22ºC in 0.5M NaCl at pH 7 and -800, -900 or -1050 mV SCE. The hydrogen diffusivity and subsurface concentration (C_0) were evaluated by fitting a fourier series expansion of the diffusion equation to the permeation data. The hydrogen diffusivity in the steel was found to be approximately 2×10^{-7} cm^2/s.

Furthermore, the influence of sulphite, dithionite, thiosulphate and sulphide on hydrogen uptake in 520M were studied at -800, -900, and -1050 mV at two different concentrations (10 or 100 mM in 0.5M NaCl) and pH 7 in the charging cell solution. Generally, sulphur components were found to increase the hydrogen permeation rate, basically with one exception. The hydrogen permeation rate was found to be reduced at -800 mV when thiosulphate was present in the solution. The increased hydrogen permeation rate is assumed to be caused by an increase in C_0, which was found to increase when the sulphur compounds were present in the charging cell solution. The highest increase in C_0 was found for solutions containing sulphide. The sulphur species are believed to poison the steel surface which increases the chemical potential of adsorbed hydrogen on the surface.

Keywords: Hydrogen diffusion; Sulphur compounds; Carbon steel; Cathodic protection.

1. INTRODUCTION

Hydrogen dissolved in metals and alloys can cause detrimental effects on metallurgical and mechanical properties [1–6]. The effects are often referred to as hydrogen embrittlement and hydrogen blistering. Hydrogen embrittlement is a collective name for a number of different mechanisms, and therefore making it sometimes a rather confusing subject. High-strength alloys are often susceptible to one form of hydrogen embrittlement called hydrogen induced cracking (HIC) or hydrogen-induced

stress cracking (HISC). The cracking mechanism involved in HIC is however a matter of much debate since none of the proposed mechanisms has been generally accepted [7].

Lower-strength stainless steels of high ductility may also experience a reduction in tensile ductility but are generally free from HIC. In low-alloy and carbon steel weldments one can find a form of HIC called underbead cracking. Rapid cooling of various carbon and low-alloy steels in the partially melted unmixed zone of the weldment produces martensite structures that are susceptible to HIC. Prevention requires careful selection of base-and weld-metal hardenability, cooling rate, and postweld treatment to keep hardness below specific levels. This became very evident at the Åsgard oil field during some failures in subsea oil and gas pipelines in the North Sea. The failures occurred as cracks at welds between low-alloyed carbon steel and 13Cr stainless steel tubes. In this case it was suspected that the failures could be explained by a combination of precipitation of brittle martensite in the heat affected zone of the weld, and hydrogen originating from cathodic protection of the carbon steel [8,9]. These problems has also led to new concepts when applying cathodic protection to offshore pipelines [10]. However, to be able to reduce the risk for hydrogen damage it is necessary to gain knowledge of the processes involved in the hydrogen uptake, and not only concentrate on the effects of hydrogen in materials. It is therefore important to investigate which factors that increase the hydrogen uptake in order develop new methods and standards to prevent hydrogen damage in the future.

The influence of H_2S on the cracking resistance as well as hydrogen permeation is previously investigated [11–14], and it is known that H_2S increases hydrogen absorption in steels probably due to a poisoning effect from HS^- on the surface [15,16]. However, many different theories describing the mechanism involved in the increased hydrogen absorption due to the surface poisons have been proposed [17,18]. The increase in hydrogen absorption obviously increases the subsurface hydrogen concentration, C_0, and hence also the permeation rate. Knowledge about how different conditions influence C_0 is vital for the ability to estimate the risk for hydrogen related damages in different systems. Albeit being some of the most studied electrochemical processes, H electroadsorption and electroabsorption are far from being well-understood at the atomic level [19].

The purpose of the present study was to investigate the effect of SO_3^{2-} (sulphite), $S_2O_4^{2-}$ (dithionite), $S_2O_3^{2-}$ (thiosulphate), and S^{2-} (sulphide) on hydrogen uptake and permeation in 520M at three different cathodic potentials. Hydrogen concentrations and diffusivities in the steel membranes have been estimated by curve fitting a simple theoretical model to the experimental permeation data. The effect of the sulphur compounds are compared by evaluating the respective values for C_0.

2. EXPERIMENTS

In the present study the Devanthan–Stachurski permeation cell was used to study hydrogen diffusion in 520M carbon steel [20]. A schematic view of the permeation cell is presented in Fig. 1.

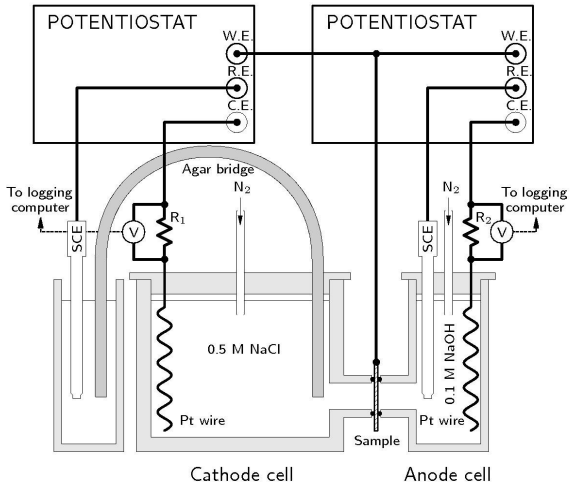

Figure 1. Schematic view of the permeation cell.

2.1. Equipment

The equipment consisted of two potentiostats, one 8-channel Gamry multiplexer connected to a computer with logging software, and the permeation cell itself. The two cells in the permeation equipment were made of polytetrafluorethylene (Teflon) and the lids were made of Plexiglass. The reference electrodes were standard Saturated Calomel Electrodes (SCE) and platinum wires with an exposed area of 4.5 cm^2 were used as counter electrodes. Rubber rings with a diameter of 16 mm sealed the connection between the sample and the cells leaving approximately 2.0 cm^2 of the sample exposed to the electrolytes in each cell. An agar bridge connected one of the reference electrodes to the cathode cell. The agar bridge was used to eliminate the risk of sulphur contamination of the reference electrodes during experiments.

The current in each cell were measured by logging the potential over the resistors (R1 = 5000 Ω and R2 = 50 000 Ω) at applied potential once every 120 s by two channels from the multiplexer. The data was stored in the computer. By using two permeation cells, four potentiostats, and four channels on the multiplexer, two separate measurements could be performed simultaneously.

2.2. Sample preparation

Samples were cut from a 25 mm diameter 520M steel bars. The chemical composition of the steel is presented in Table 1. The samples were polished with SiC paper down to 1000 mesh, degreased in ethanol and dried in air. The thickness of the samples after polishing was 1 mm. One side of each sample was coated with Pd in a sputter coater. The thickness of the Pd film was approximately 1μm. Finally the sample was mounted in the permeation cell with the coated side facing the anode (exit) cell.

Table 1. Chemical composition of 520M carbon steel. (From inspection certificate).

C	Si	Mn	P	S	V	Fe
0.14	0.36	1.12	0.014	0.034	0.05	Balance

2.3. Experimental procedure

When the sample had been mounted in the permeation cell the oxidation (exit) cell was filled with 0.1M NaOH and nitrogen purging was commenced immediately after filling the cell. When all cables and electrodes were connected properly a potential of +300 mV SCE was applied to the sample and two minutes later the logging program was started. The equipment was left for 24 hours until a low and stable background signal had been reached. Then the charging (entrance) cell was filled with the test solution, the sample polarized to -800, -900 or -1050 mV SCE, and nitrogen purging started. The measurement was stopped 20 hours later when steady state diffusion was considered established.

Nine different test solutions with different concentrations of various sulphur compounds were evaluated. One 0.5M NaCl reference solution, 0.5M NaCl with 10mM or 100mM of either sulphite, dithionite, thiosulphate, or sulphide. All base solutions of 0.5M NaCl were nitrogen purged for 30 minutes before addition of sulphur compounds. Hydrochloric acid or sodium chloride were added all solutions in order to adjust pH to approximately 7 before adding them to the permeation cell. After each experiment the pH in the charging cell was also measured. See Table 2 for a compilation of the measured pH in the charging cell before and after each measurement.

All experiments were performed at room temperature.

Table 2. pH in charging cell measured before and after experiment.

	pH (Before/After)		
Potential (mV SCE)	**-800**	**-900**	**-1050**
0mM			
Non added	7.01/6.80	6.99/6.94	7.01/6.95
10mM			
SO_3^{2-}	7.03/5.05	7.02/6.14	7.02/5.03
$S_2O_4^{2-}$	6.94/6.21	6.82/7.06	6.65/6.34
$S_2O_3^{2-}$	7.03/6.47	7.00/6.27	7.01/6.75
S^{2-}	7.83/9.64	7.17/9.02	7.24/9.44
100mM			
SO_3^{2-}	7.15/6.82	7.13/6.68	7.03/6.92
$S_2O_4^{2-}$	6.82/6.44	7.01/6.43	6.76/6.21
$S_2O_3^{2-}$	7.06/6.98	7.08/7.53	7.02/7.96
S^{2-}	6.73/6.73	6.99/7.48	7.02/8.37

3. RESULTS AND DISCUSSION

In this section the experimental results are presented. The results are discussed in view of a suggested surface poison effect by the sulphur compounds and an eventual retarding effect on the hydrogen absorption by sulphide film formation.

3.1. Theoretical model

The following assumptions were made to derive a theoretical model for the hydrogen diffusion through the steel membrane. First it is assumed that the sample is effectively emptied of any residual hydrogen during the first 24 hours when the sample is polarized to +300 mV at the exit side with no solution in the charging cell. The initial hydrogen concentration in the steel membrane is therefore set to zero in the model. The boundary conditions are assumed to be constant and $C(0,t)=C_0$ at the entrance side and $C(L, t)=0$ at the exit side for $t \geq 0$. The time when the cathodic potential is applied to the sample in the charging cell is defined as $t = 0$ in the model. The initial condition and the boundary conditions give the following expression for the hydrogen flux,

$$J(x,t) = \frac{DC_0}{L} + \frac{2DC_0}{L}\sum_{n=1}^{\infty}\cos\frac{n\pi x}{L}e^{-n^2\pi^2 Dt/L^2} \qquad (1)$$

where $J(x, t)$ is the flux, D is the diffusivity, C_0 is the subsurface H concentration, and L is the membrane thickness [21].

3.2. Curve fitting

Eq. (1) was used to fit curves to the experimental data for the hydrogen flux at the exit side $(x = L)$. GnuPlot 4.0 was used for curve fitting with D and C_0 as variables and the fit included the terms $n = 1$ to 49 in the sum. In general a summation of the terms $n = 1$ to 6 is sufficiently accurate [22], but since the fits converged quite fast more terms were used. Fig. 2 show two sets of experimental data and respective curve fit. All fitted parameters, D and C_0, for the different potentials and solutions are listed in Table 3.

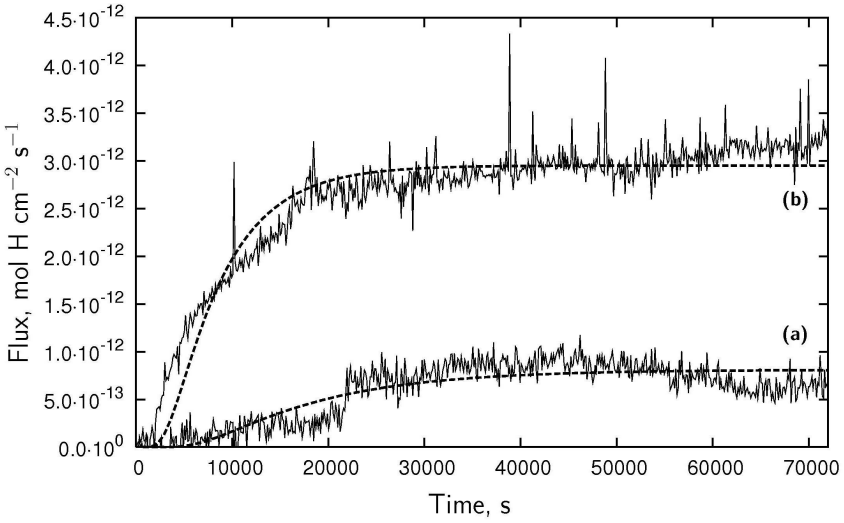

Figure 2. Experimental permeation data and curve fits at -800 mV for (a) 0.5M NaCl and (b) 0.5M NaCl with 10mM sulphite.

Table 3. Hydrogen diffusivities and subsurface hydrogen concentrations estimated from curve fitting to experimental permeation data.

	Potential (mV SCE)					
	-800	-900	-1050	-800	-900	-1050
	D x 10^7 (cm^{-2}/s)			**C_0 x10^7 (mol H/cm^3)**		
0 mM						
Cell 1	0.8	4.0	0.9	9.2	2.6	27.4
Cell 2	2.0	2.4	1.1	3.2	3.8	20.8
10 mM						
SO_3^{2-}	1.6	1.5	2.8	16.5	59.4	24.7
$S_2O_4^{2-}$	2.2	3.9	0.9	11.4	20.8	264.2
$S_2O_3^{2-}$	-	1.6	2.2	-	4.1	20.1
S^{2-}	-	1.7	2.4	.	83.7	98.3
100 mM						
SO_3^{2-}	1.7	2.7	5.6	12.4	39.8	78.0
$S_2O_4^{2-}$	-	3.7	2.9	-	28.5	112.6
$S_2O_3^{2-}$	-	0.9	3.0	-	34.4	14.7
S^{2-}	5.3	2.5	11.1	20.7	216.2	52.7

In some of the permeation curves, a maximum in the flux was recorded before a decrease to a lower steady state value occurred. In those cases the curve fit was performed on the data up to the maximum flux value. In this way the highest value of the subsurface concentration is found representing the worst case. The maximum can have many different causes. Hydrogen bubbles formed on the surface of the sample reduces the area exposed to the electrolyte, which decreases the hydrogen flux into the sample. Another explanation is that cavities are formed in the bulk of the sample. These cavities both traps hydrogen and also makes the diffusion path more tortuous [23]. This effect alters the apparent diffusivity for hydrogen in the sample. The effect of tortuosity have previously been discussed for hydrogen diffusion in duplex stainless steels, where the fast diffusion occurs in the α-phase and the γ-phase causes the tortuosity due to a low diffusivity value in this phase [24,25]. Other studies have shown that hydrogen charging can increase the dislocation density and also cause grain refinement in ferrite [3,4]. These two effects might also contribute to a lower apparent diffusivity and a lower flux.

Furthermore, film growth on the sample surface can reduce the hydrogen flux [26,27].

3.3. Addition of Sulphur Species

The values of D and C_0 producing the best curve fits to the experimental data are presented in Table 3. It is seen that the values for D is in the range $0.7 \times 10^{-7} - 11.1 \times 10^{-7}$ cm^2/s, which is in agreement with values reported elsewhere for hydrogen diffusion in ferritic structures at room temperature [25,28–31]. Furthermore the data in Table 3 show that the hydrogen concentration generally increases when the sulphur compounds are present with only some exceptions at -800 mV.

The exceptions are marked with dots in the table and indicate experiments where no increase in the hydrogen permeation rate could be detected compared to the permeation rate in reference solution. Due to background noise no reliable data were attained for the experiments with 10mM sulphide at -800 mV and 100mM dithionite at -800 mV. For thiosulphate the permeation current vanished at -800 mV. A plausible explanation to this is presented below.

The steady state flux of hydrogen through the sample is given by Eq. (1) as $j(x,\infty) = DC_0/L$. In our case the steady state flux only depends on the product DC_0 since all samples had the same thickness (L =1 mm). However, it is reasonable to assume that the diffusivity in the different samples were approximately the same because they all originate from the same steel bar and have been treated in the same way. Therefore we normalize our data for C_0 to a common value for D instead of the values giving the best curve fits.

So, to be able to range the different sulphur compounds in their respective ability to increase C_0 we choose to set the diffusivity to the mean value of the measured diffusivity with reference solution (0.5M NaCl), $D = 1.9 \times 10^{-7}$ cm^2/s, for comparative reasons. It is now possible to compare the different sulphur compounds in a qualitative way by recalculating the concentration values in Table 3 with the following formula,

$$C'_0 = \frac{D}{D'} \cdot C_0 \tag{2}$$

The result of applying Eq. (2) on the data in Table 3 is presented in Table 4. The first thing that is now seen is that the subsurface hydrogen concentration increases with increasing cathodic potentials, which should be expected in the present potential region. Based on the results in Table 4, that the C'_0-value for dithionite increases typically by a factor of 3 when the cathodic potential is increased 100 mV in the examined region, it seems like a reasonable estimate that the concentration should be somewhere around 20×10^{-7} mol H/cm^3 at -800 mV in 0.5M NaCl with 100mM dithionite. A similar estimation of C'_0 for sulphide at 10mM and -800 mV would also be somewhere around 20×10^{-7} mol H/cm^3. It should be noted that there is probably a quite large error in the presented concentration values but that they likely presents a reliable comparison between the effect of the different sulphur compounds.

The following three main reactions of the examined sulphur compounds have been proposed elsewhere [32].

$$SO_3^{2-} + 6H^+ + 6e^- = S^{2-} + 3H_2O \tag{3}$$

$$S_2O_4^{2-} + 8H^+ + 10e^- = 2S^{2-} + 4H_2O \tag{4}$$

$$S_2O_3^{2-} + 6H^+ + 8e^- = 2S^{2-} + 3H_2O \tag{5}$$

In addition to these three reactions dithionite is also reported to disproportionate into sulphite and sulphide according to

$$3S_3O_4^{2-} + 3H_2O = S^{2-} + 5SO_3^{2-} + 6H^+ \tag{6}$$

For simplicity sulphide is expressed as S^{2-} in Eqs. (3)–(6) although they exist in equilibrium mainly as HS^- and H_2S at pH 7. It is seen that all reactions produce sulphide ions which will form HS^- or H_2S.

Table 4. Hydrogen subsurface concentrations, C'_0 calculated based on assumed hydrogen diffusivity of 1.9×10^{-7} cm^2/s in the steel sample.

	C´$_0$ x 10^7 (mol H/cm^3)		
Potential (mV SCE)	**-800**	**-900**	**-1050**
0mM			
Cell 1	3.9	5.5	13.0
Cell 2	3.4	4.8	12.0
10mM			
SO_3^{2-}	13.9	46.9	36.4
$S_2O_4^{2-}$	13.2	42.7	125.1
$S_2O_3^{2-}$	-	3.5	23.3
S^{2-}	-	74.9	124.2
100mM			
SO_3^{2-}	11.1	56.6	229.9
$S_2O_4^{2-}$	19.0	55.5	171.9
$S_2O_3^{2-}$	-	16.3	23.2
S^{2-}	57.7	284.7	307.9

Table 4 show similar values for sulphite and dithionite indicating that these two compounds have a similar impact on the hydrogen absorption rate. This result may be explained by the disproportion reaction shown in Eq. (6) producing sulphite, which subsequently is reduced according to Eq. (3). Sulphite and dithionite increases the hydrogen absorption at all examined potentials. The data reveals no clear tendency for higher hydrogen permeation with increased concentrations of sulphite or dithionite at the charging side.

For thiosulphate on the other hand, no significant permeation current could be detected at -800 mV for both concentrations even though the background current was low and stable. It therefore seems possible that thiosulphate retards hydrogen absorption at -800 mV. It is also seen that all C'_0-values for thiosulphate are much smaller compared to the values for the other compounds. A possible explanation to the reduced hydrogen absorption is that an iron sulphide film is formed on the surface. The charged sides of the samples were black after the 24-hour exposure at -800 mV. After exposure at -900 or -1050 mV the surface appeared slightly grey. Pourbaix diagrams of Fe in thiosulphate solution show that the FeS film is thermodynamically stable at -800 mV but that it's not favoured at higher cathodic potentials [33]. The stability limit for FeS at pH 7 is very close to -900 mV indicating that film formation may explain the low C'_0-values at this potential as well. However, any reason why thiosulphate should produce a more protective FeS film than the other compounds cannot be found. At -1050 mV thiosulphate clearly increases the hydrogen uptake, but not to the same extent as the other compounds.

Another reason for the low C'_0-values for thiosulphate may be that the reaction presented in Eq. (5) is not dominating in our measurements. Instead another reaction is proposed [34].

$$S_2O_3^{2-} + H_2O = HS^- + SO_4^{2-} + H^+ \quad (7)$$

Thiosulphate is suggested to decompose according to Reaction 7 in neutral solution when a cathodic polarization is applied. The reduced hydrogen absorption may then be explained by adsorption of sulphate (SO_4^{2-}) on the metal surface and that the sulphate favours the hydrogen evolution reaction or blocks favourable sites where hydrogen can enter into the subsurface region. This is opposite to the effect of HS^-. Other studies have also shown that adsorbed sulphate has an appreciable influence on the formation of calcareous deposits during cathodic protection [35]. In solutions containing SO_4^{2-} the deposition of aragonite ($CaCO_3$) was slower and that parts of the surface stayed uncovered.

Sulphide is shown to increase the hydrogen absorption at all present potentials. Increasing the sulphide concentration from 10 to 100mM also increases the hydrogen uptake significantly.

3.4. Poison effect

It is well known that adsorption of catalyst poisons, such as hydrogen sulphide, thiourea, arsenic compounds, etc., promotes the cathodic sorption of H into host metal lattices, such as Fe, Ti, Pd or Ni. Many different mechanisms for the promotion of hydrogen sorption by surface poisons have been discussed by various authors and the following summary of the different ideas have been presented as [17,26]: (a) additives such as Sb or As promote the hydrogen sorption by formation of (gaseous) hydrides; (b) the poisons increase the M–H bond strength; (c) 'colloidal particles', formed during electrolysis, promote entry of H; (d) in the presence of poisons, H can enter the host metal as injected protons; (e) poisons interfere with the H atom recombination step in cathodic H_2 evolution, thereby supposedly increasing the probability of H entry.

Usually, it is supposed that poisons block H + H recombination to H_2 and thus favour entry of adsorbed H into the metal. However, this explanation seems ambiguous since poisons are also known to reduce θ_H owing to competition between poison and H for surface sites. The proposed mechanism of poisons as recombination blockers is therefore not entirely conclusive. A thermodynamic theory for the enhancement of H sorption by poisons including competitive adsorption have been proposed elsewhere [17,18]. The theory explains how coadsorption of H and poisons increases the chemical potential of adsorbed H. The change in chemical potential for H when poisons are present compared to when they are absent is shown to be

$$\delta\mu = \mu^0_{H(P)} - \mu^0_H + RT\ln(1 + K_P C_P) \quad (8)$$

where K_P is the chemical adsorption constant, and C_P is the concentration of the poison in the solution respectively. Since the driving force for sorption depends on the chemical potential of H at the surface it is shown that the enhanced hydrogen sorption can arise from fundamental thermodynamical reasons.

This does however not support our suggestion that adsorption SO_4^{2-} decreases the hydrogen uptake. On the other hand, the data presented in this work indicate that the compound that is most prone to produce the HS^- anion also produces the highest increase in hydrogen absorption.

4. CONCLUSIONS

The conclusions based on the data from this experimental campaign are presented below.

- The simple diffusion model based on Fick's second law can be used to simulate hydrogen diffusion in steel 520M exposed to 0.5M NaCl and polarized to -800 to -1050 mV.
- The diffusion coefficient for H in 520M is approximately 1.9×10^{-7} cm^2/s at 22ºC.
- The hydrogen uptake is generally higher when sulphur components are present at the charging side.
- It is possible that iron sulphides formed at -800 mV reduces hydrogen absorption in the steel.
- The ability of the four different sulphur compounds to increase hydrogen absorption can be ranged as follows; $S_2O_3^{2-} < SO_3^{2-} \approx S_2O_4^{2-} < S^{2-}$.

References

1 Q. Yang and J. Luo, *Mat. Sci. Eng.* A288 (2000) 75.
2 O. El kebir and A. Szummer, *Int. J. Hydrogen Energy,* 27 (2002) 793.
3 A. Głowacka and W. A. Swiątnicki, *Mat. Chem. Phys.*, 81 (2003) 496.
4 A. Głowacka and W. Swiątnicki, *J. Alloys Comp.,* 701 (2003) 356-357.
5 M. Hoelzel, S. Danilkin, H. Ehrenberg, D. Toebbens, T. Udovic, H. Fuess, and H. Wipf, *Mat. Sci. Eng.,* A384 (2004) 255.
6 M. Wozniak, A. Glowacka, and J. Kozubowski, *J. Alloys Comp.* 404-406, 626 (2005).
7 D. Jones, *Principles and Prevention of Corrosion*, Macmillan Publishing Company, 1992.
8 K. Førre, T. Hemmingsen, and S. Eliassen, Report (in Norwegian), Stavanger University College, 2003.
9 T. Hemmingsen, K. Førre, H. Urke, N. Aagotnes, and S. Eliassen, *in Proceedings, 13th Scandinavian Corrosion Congress,* Iceland, 2004.
10 S. Eliassen, *Corr. Eng. Sci. Tech.*, 39 (2004) 31.
11 K. Sieradzki, *Scripta Metall.*, 15 (1981) 171.
12 M. Saenz de Santa Maria and A. Turnbull, *Corr. Sci.*, 29 (1989) 69.
13 A. Turnbull, M. Saenz de Santa Maria, and N. Thomas, *Corr. Sci.*, 29 (1989) 89.
14 D. Seeger and T. Boellinghaus, *in Corrosion 2003,* (NACE International, 2003) paper No. 03098.
15 U. Evans, *The Corrosion and Oxidation of Metals,* Edvard Arnold (Publishers) Ltd., 1976, chap. 11, p. 218.
16 T. Zakroczymski, *Hydrogen Degradation of Ferrous Alloys,* Noyes Publications, Park Ridge (1985).
17 B. Conway and G. Jerkiewicz, *J. Electroanal. Chem.*, 357 (1993) 47.
18 G. Jerkiewicz, J. Borodzinski, W. Chrzanowski, and B. Conway, *J. Electrochem. Soc.*, 142 (1995) 3755.
19 G. Jerkiewicz, *Prog. Surf. Sci.*, 57 (1998) 137.
20 M. Devanathan and Z. Stachurski, *Proc. Roy. Soc.*, A270 (1962) 90.
21 J. Crank, *The Mathematics of Diffusion*, Oxford University Press, (1957).

22 T. C. ISE/NFE/8, *Method of Measurement of Hydrogen Permeation and the Determination of Hydrogen Uptake and Transport in Metals by an Electrochemical Technique*, British Standard, BS7886:1997 (1997).
23 J. Bockris, M. Genshaw, and M. Fullenwider, *Electrochimica Acta,* 15 (1970) 47.
24 E. Lembach-Beylegaard, *Ph.D. thesis*, Norges teknisk-naturvitenskapelige universitet, NTNU (1996).
25 E. Owczarek and T. Zakroczymski, *Acta Mater.*, 48 (2000) 3059.
26 T. Radhakrishnan and L. Shreir, *Electrochimica Acta,* 11 (1966) 1007.
27 S. Yen, *Met. Chem. Phys.*, 59 (1999) 210.
28 T. Radhakrishnan and L. Shreir, *Electrochimica Acta*, 12 (1967) 889.
29 L.-C. Hwang and T.-P. Perng, *Mat. Chem. Phys.*, 36 (1994) 231.
30 A. Turnbull and R. Hutchings, *Mat. Sci. Eng.*, A177 (1994) 161.
31 S. Serna, H. Martínez, S. López, J. González-Rodríguez, and J. Albarrán, *Int. J. Hydrogen Energy,* 30 (2005) 1333.
32 T. Hemmingsen, F. Fusek, and E. Skavås, *Electrochimica Acta*, 51 (2006) 2919.
33 P. Marcus and E. Protopopoff, *Corr. Sci.*, 39 (1997) 1741.
34 R. Hu, P. Manolatos, M. Jerome, M. Meyer, and J. Galland, *Corr. Sci.*, 40 (1998) 619.
35 C. Barchiche, C. Deslouis, O. Gil, P. Refait, and B. Tribollet, *Electrochimica Acta*, 49 (2004) 2833.